Title

Near-infrared imaging of secondary caries lesions around composite restorations at wavelengths from 1300–1700-nm

Journal

Dental Materials, 32(4)

ISSN

0109-5641

Authors

Simon, Jacob C
Lucas, Seth A
Lee, Robert C
et al.

Publication Date

2016-04-01

DOI

10.1016/j.dental.2016.01.008

Peer reviewed

HHS Public Access

Author manuscript

Dent Mater. Author manuscript; available in PMC 2017 April 01.

Published in final edited form as:

Dent Mater. 2016 April ; 32(4): 587–595. doi:10.1016/j.dental.2016.01.008.

Near-infrared Imaging of Secondary Caries Lesions around Composite Restorations at Wavelengths from 1300–1700-nm

Jacob C. Simon, **Seth Lucas**, **Robert Lee**, **Cynthia L. Darling**, **Michal Staninec**, **Ram Vanderhobli**, **Roger Pelzner**, and **Daniel Fried**

University of California, San Francisco, San Francisco, CA 94143-0758

Abstract

Background and Objectives—Current clinical methods for diagnosing secondary caries are unreliable for identifying the early stages of decay around restorative materials. The objective of this study was to access the integrity of restoration margins in natural teeth using near-infrared (NIR) reflectance and transillumination images at wavelengths between 1300–1700-nm and to determine the optimal NIR wavelengths for discriminating composite materials from dental hard tissues.

Materials and Methods—Twelve composite margins (n=12) consisting of class I, II & V restorations were chosen from ten extracted teeth. The samples were imaged *in vitro* using NIR transillumination and reflectance, polarization sensitive optical coherence tomography (PS-OCT) and a high-magnification digital microscope. Samples were serially sectioned into 200–μm slices for histological analysis using polarized light microscopy (PLM) and transverse microradiography (TMR). Two independent examiners evaluated the presence of demineralization at the sample margin using visible detection with 10× magnification and NIR images presented digitally. Composite restorations were placed in sixteen sound teeth (n=16) and imaged at multiple NIR wavelengths ranging from λ=1300–1700-nm using NIR transillumination. The image contrast was calculated between the composite and sound tooth structure.

Results—Intensity changes in NIR images at wavelengths ranging from 1300–1700-nm correlate with increased mineral loss measured using TMR. NIR reflectance and transillumination at wavelengths coincident with increased water absorption yielded significantly higher ($P<0.001$) contrast between sound enamel and adjacent demineralized enamel. In addition, NIR reflectance exhibited significantly higher ($P<0.01$) contrast between sound enamel and adjacent composite restorations than visible reflectance.

Significance—This study shows that NIR imaging is well suited for the rapid screening of secondary caries lesions.

Corresponding author: Dr. Daniel Fried, Department of Preventive and Restorative Dental Sciences, University of California, San Francisco, San Francisco, CA 94143-0758, daniel.fried@ucsf.edu, Phone: 415-502-6641, Fax: 415-476-0858.

Keywords

secondary caries; composite restorative materials; near-IR imaging; optical coherence tomography

1. Introduction

Secondary (recurrent) caries is the major etiologic factor in the failure of dental restorations, and dentists spend more time replacing restorations than placing new ones [1, 2]. Conventional clinical methods for evaluating demineralization surrounding restorations rely upon visible inspection for discoloration and gaps/microleakage, and tactile sensation with an explorer or periodontal probe. It is clear from clinical data that neither discoloration nor ditching (for gap distances <500-μm, which are considerable) is a consistent indicator of the integrity of the enamel or dentin, and a considerable number of restorations are unnecessarily replaced using such criteria [2–7]. Inspection via tactile examination also presents the risk of accelerating decay by damaging the protective lesion surface zone. New imaging methods that can discriminate between sound enamel, demineralized enamel and composites with higher diagnostic performance for secondary caries lesions are needed.

To address this need, optical techniques including digital radiographs (X-rays), quantitative laser fluorescence (QLF, collagen fluorescence), and red laser fluorescence (LF, porphyrin fluorescence) have been investigated as alternative, nondestructive approaches for diagnosing recurrent decay, albeit that each modality has significant limitations.

Digital radiographs lack the sensitivity to detect changes present during the early stages of lesion progression. Generating radiographic images requires ionizing x-rays and a direct viewing angle of the interproximal regions to produce a diagnostic image [8]. When imaging restored teeth, amalgam and composite restorations are radiopaque and may mask the presence of caries either partially or completely which contributes to the difficulty of diagnosis, and therefore are poorly suited for detecting secondary caries [9–13].

Quantitative light fluorescence (QLF) uses UV or blue light ranging from 370–470-nm in wavelength to excite the proteins in enamel and dentin, and identifies lesions by measuring the loss of fluorescence at wavelengths >500-nm (green light) [14–16]. Measuring lesion severity based on a loss of signal with visible light is problematic due to the high absorption from stain that attenuates light and results in false positives using this method. Secondary caries detection using QLF has been comparable in accuracy to visual diagnosis [13, 17, 18].

Laser fluorescence (LF) uses ~655-nm light to excite fluorescence of bacteria-produced porphyrins and measures light emission at wavelengths >680-nm (near-infrared) [19, 20]. In LF, the presence of a fluorescent signal is used to locate infected areas as a function of bacteria concentration and studies suggest that LF out performs visible and QLF methods for the detection of recurrent decay [13, 17, 18, 21–23]. Unfortunately, LF is prone to false positives due to poor correlation between porphyrin concentration and lesion severity and requires cleaning of tooth surfaces for effective use. Furthermore, the excitation wavelengths used in LF has been shown to cause fluorescence in many dental restorative materials, including some sealants [24, 25]. For LF devices such as the DIAGNOdent, this requires the

user to continually calibrate the device against a ceramic standard, and against sound enamel for each individual tooth [13].

Near-infrared (NIR) imaging, has the potential for improved performance over current methods used to detect recurrent decay by illuminating and capturing images of tooth structures formed by deeply penetrating, non-ionizing light ranging from 700–1700-nm in wavelength. Compared to visible light, light scattering in sound enamel at λ=1300-nm is ~20×–30× less making sound enamel virtually transparent [26]. When sound enamel becomes demineralized by caries, pores within the lesion grow to a similar size of the wavelength of light and act as Mie scatters increasing the scattering coefficient 2–3 orders of magnitude [27]. Differences in light scattering between sound and demineralized enamel can be detected by imaging light transmitted through or reflected back from the tooth [28]. Imaging with longer wavelength (λ≥1300-nm) NIR light also avoids the absorption bands of organic molecules responsible for pigmentation allowing direct imaging of decay beneath stained surfaces such as the occlusal grooves [29]. Additionally, composite restorative materials have unique spectral signatures in the NIR resulting from combination absorption bands that can be exploited for differentiating tooth structure and other type of composites. The most prominent dental resin absorption bands lie at 1171, 1400, 1440, 1620 and 1700-nm and result from overtones and combinations of the fundamental mid-IR vibrational bands from C-H, N-H, and O-H groups found in both resin and water [30–32].

Recent studies have investigated the use of polarization sensitive optical coherence tomography (PS-OCT), at ~1300-nm, for the detection of demineralization beneath sealants and composites in addition to primary lesions [33–36]. These studies demonstrated the ability of PS-OCT to produce three-dimensional data sets that accurately indicate demineralized tissue surrounding restorations. Furthermore, PS-OCT can be used to calculate the integrated reflectivity with depth of the tissue, ΔR, a physical quantity that directly correlates with ΔZ, the integrated mineral loss with depth, and the gold standard for lesion severity. Although PS-OCT is a powerful imaging technique, the vast amounts of data produced from each scan and inherent difficulty of presenting and comprehending three-dimensional data sets make it poorly suited as a caries-screening tool. Another challenge is that the scanning area is relatively small compared to the size of the tooth such that you cannot ‘see’ the entire tooth anatomy, and increasing the scanning area increases the size of the data set and computational burden.

NIR two-dimensional imaging modalities have demonstrated high image contrast for early surface demineralization using NIR reflectance at λ=1460-nm and NIR transillumination at λ=1300-nm [37–41]. Many composite restorative materials are translucent to NIR light and allow demineralization to be imaged directly through the restorations [42, 43]. Additionally, the overall visualization of the restoration boundaries can be enhanced when viewed at different NIR wavelengths [44]. A technique with these abilities should be ideally suited for the detection of recurrent caries in both planes; the surface enamel and the enamel of the cavity wall as defined by [3]. These caries affected planes are classified as either *outer lesions*, primary lesions that develop from the surface adjacent to the restoration, or *wall lesions*, decay along the enamel of the cavity as a result of microleakage or ditching. With the advantage of real-time video acquisition and presentation with simple interpretation,

NIR imaging is poised to be a viable rapid screening tool for secondary caries and restoration monitoring.

Currently, the major factor limiting the use of NIR techniques in dentistry is the cost of the NIR sensitive camera sensors. With increased interest in NIR imaging for dental and other medical applications, these costs are projected to decrease.

The objective of this study was to calculate the lesion contrast in NIR reflectance and NIR transillumination images of natural recurrent decay and compare that contrast with changes in tissue mineral density to determine the optimal wavelengths for imaging secondary caries. NIR images were acquired of extracted teeth with composite restorations and preexisting natural secondary caries lesions with an InGaAs camera. These images were compared with PS-OCT 2D (⊥) integrated reflectivity C-scan projections, PS-OCT (⊥) B-scans, and visible images. Polarized light and transverse microradiography images were obtained from thin sections produced by serial sectioning with a diamond saw. Normalized NIR cross-polarized reflectance and NIR transillumination image line profiles were overlaid with TMR percent mineral line profiles across the region of interest for each sample. In addition, multispectral NIR transillumination images were acquired of newly placed 3M Z250 composite restorations in extracted sound teeth to identify the NIR wavelengths that provide the highest contrast of composites relative to sound enamel.

2. Materials and Methods

2.1 Sample preparation

Twenty-eight teeth were collected from patients in the San Francisco Bay area without patient identifiers (exempt from approval by UCSF Committee on Human Research). The teeth were sterilized using gamma radiation and stored in a 0.1% thymol solution to maintain tissue hydration and prevent bacterial growth. Twelve composite margin segments (n=12) were selected from teeth with existing composite restorations for NIR imaging. Sixteen sound posterior extracted teeth (n=16) were then drilled on one side using a high-speed dental burr and filled with Z250 composite (3M, Minneapolis, MN).

A CO_2 laser (Impact 2500, GSI Lumonics Rugby, UK) was used to produce small incisions on extracted teeth forming the outline of a 4×4-mm square around the region of interest (ROI) and served as fiducial marks for PS-OCT scans. The laser was modified to produce a Gaussian output beam (single spatial mode) and pulse duration of between 10–15-μs at a wavelength of 9.3-μm. A planoconvex ZnSe lens with 90-mm focal length was used to focus the laser beam to a spot size of around ~200-μm and fluence of 20 J/cm^2. Individual laser spots were scanned using a pair of XY actuators (Newport 850G) at 50-μm increments with an automated water spray directed to the surface of the tooth to prevent peripheral thermal damage.

After all images were acquired, the samples were serially sectioned into ~200-μm thick slices using a linear precision saw, Isomet 5000 (Buehler, Lake Buff, IL) perpendicular to the restoration margin. Thin sections were subjected to histological examination with polarized light microscopy and transverse microradiography.

2.2 High Resolution Digital Microscopy

Images were taken of the region of interest on each tooth surface using a digital microscopy/3D surface profilometry system, the VHX-1000 from Keyence (Elmwood, NJ) outfitted with the VH-Z25 lens (magnification from 25–175×). Depth composition images (DCDM) were generated by translating the image plane of the objective along the vertical axis capturing a series of images containing all points of the tooth surface in optimum focus, followed by construction of an optimized 2D image using only in focus image regions from the series.

The lesion contrast measurements from visible light images where calculated by averaging the pixel values taken from a ROI approximately 25 × 25-pixels from areas of sound enamel, demineralized enamel and the composite regions. The contrast of the decay relative to both the adjacent sound enamel and restorations were calculated using the formula $(I_L\text{-}I_{S/C})/I_L$, where I_L represents the lesion intensity and $I_{S/C}$ represents either the intensity from the sound or composite regions. The image contrast varies from 0 to 1 with 1 being very high contrast and 0 having no contrast.

2.3 NIR Transillumination and NIR Cross-Polarized Reflectance

A high sensitivity, InGaAs, camera (SU320-KTSX-1.7RT/RS170) from Sensors Unlimited (Princeton, NJ), with a 320 × 256 pixel focal plane array and 25-μm pixel pitch was used to capture NIR cross-polarized (CP) reflectance, cross-polarized interproximal transillumination and occlusal transillumination images. CP-reflectance images were acquired using polarized light from a tungsten halogen lamp (E Light) and capturing the reflected signal through an orthogonal linear polarizer, long pass 1500–1700-nm optical filter and lens system. CP-interproximal transillumination images were acquired by focusing (40-mm NIR AC ThorLabs, Newton, New Jersey) polarized light from a tungsten halogen lamp laterally onto the sample and collecting the transmitted signal through an orthogonal linear polarizer, band pass 1300-nm optical filter (Spectragon, FWHM=80-nm) and lens system. Occlusal transillumination images utilized light from a tungsten halogen source and bifurcated fiber optic bundle equipped with two linear arrays to impart light angled apically at the cementoenamel junction from both sides of the tooth and collect transmitted signal through a band pass 1300-nm optical filter and lens system. Detailed schematics covering the geometry of each modality and theory of the resulting image contrast can be found in previous publications [28]. NIR images were analyzed using the image analysis package provided by IgorPRO software (Wavemetrics, Lake Oswego, OR). Image line profiles five pixels in width were extracted from the sample ROI across the same sample plane for NIR reflectance and transillumination images. The line profiles were normalized from 0 to 1, where 1 represents the maximum contrast value and 0 the minimum across the ROI.

The lesion contrast measurements from NIR reflectance images where calculated by averaging the pixel values taken from a ROI approximately 25 × 25-pixels from areas of sound enamel, demineralized enamel and the composite regions. The contrast of the decay relative to both the adjacent sound enamel and restorations were calculated using the formula $(I_L\text{-}I_{S/C})/I_L$, where I_L represents the lesion intensity and $I_{S/C}$ represents either the intensity from the sound or composite regions. NIR transillumination images appear in the

opposite contrast as reflectance images and are calculated using the equation $(I_{S/C}-I_L)/I_{S/C}$, where I_L represents the lesion intensity and $I_{S/C}$ represents either the intensity from the sound or composite regions. The image contrast varies from 0 to 1 with 1 being very high contrast and 0 having no contrast.

Sound-restored composite samples were imaged in transillumination at three principal wavelength bands in the NIR using band-pass (BP) filters BP-1300-90, BP-1460-85 from Spectrogon (Parsippany, NJ) and BP1550-40 from Thorlabs. A ROI, approximately 25 × 25-pixels was extracted from an occlusal surface area of sound enamel and a region within the composite and averaged to calculate the mean intensity from the respective regions I_s and I_c. Image contrast was calculated using the equation $(I_c-I_s)/I_c$. The image contrast varies from 0 to 1 with 1 being very high contrast and 0 having no contrast. The contrast was calculated for each wavelength. For teeth with composites that extended into the dentin, the same analysis was performed to calculate the image contrast between the sound dentin and composite restoration. A one-way analysis of variance (ANOVA) followed by the Tukey-Kramer post hoc multiple comparison test was used to compared groups for each wavelength employing Prism software (GraphPad, San Diego, CA).

2.4 Measures of Image Reliability

Four clinicians (2 per method) examined tooth samples using visible light or NIR images while blind to the other modality, and provided yes or no responses to the question, *does demineralized tissue exist at the restoration margin?* Visible inspection permitted the use of 10× magnification, LED lights and dental instruments to examine the extracted tooth surface. Clinicians chosen for visible inspection were trained dental educators. NIR inspection consisted of viewing 2D still images of samples obtained via transillumination or reflectance geometries on a digital display. Clinicians chosen for NIR inspection had limited experience interpreting NIR images due to the novelty of the technology.

2.5 Polarization Sensitive Optical Coherence Tomography

An all-fiber-based optical coherence domain reflectometry (OCDR) system was used with polarization maintaining (PM) optical fibers, high-speed piezoelectric fiber-stretchers and two balanced InGaAs receivers that was designed and fabricated by Optiphase, Inc., Van Nuys, CA. The two-channel system was integrated with a broadband superluminescent diode (SLD) Denselight (Jessup, MD) and a high-speed XY-scanning system (ESP 300 controller and 850G-HS stages, Newport, Irvine, CA) for *in vitro* optical coherence tomography. The high power (15-mW) polarized SLD source, emitted near-IR light at a center wavelength of 1317-nm with a spectral bandwidth full-width at half-maximum (FWHM) of 84-nm. The beam was focused onto the sample surface using a 20-mm focal length AR-coated planoconvex lens. This configuration provided lateral and axial resolutions of approximately 20-μm and 10-μm in air with a signal to noise ratio of greater than 40–50-dB. When imaging enamel tissues with refractive index $n\approx1.63$, spatial resolution is increased relative to air due to the tissues greater refractive index. The PS-OCT system is completely controlled using Labview software (National Instruments, Austin, TX).

2.6 CP-OCT Integrated Reflectivity Collapsed C-scan 2D Projections

Raw OCT data was analyzed using a program written in Labview. Co-polarization and cross-polarization (CP-OCT) OCT images were acquired for each sample, however only the cross-polarization images were processed and analyzed. For speckle noise reduction, signals not exceeding four standard deviations from the mean background noise floor were reduced to the mean background value and a Gaussian blur smoothing algorithm was applied using a 5×5 pixel convolution kernel. In the edge-detection approach, the enamel edge and the lower lesion boundary were determined by applying an edge locator. The program first locates the maximum of each a-scan, and differentiates the a-scan maximum as either demineralized or sound using the signal-to-noise ratio as a threshold. The lesion depth is calculated by locating the upper and lower lesion boundaries, calculated by determining the first pixel that does not satisfy the threshold of e^{-2} of the maximum value. The distance per pixel conversion factor was obtained experimentally by system calibration. A linear relationship was established between the OCT lesion depth and the histological depths measured using polarized light microscopy (PLM). Based on this relationship, a linear correction was applied to the lesion depth calculated from OCT (Corrected Pixel Depth = (1.55 × Measured OCT pixel depth) – 37.6) [45].

Each A-scan of the CP-OCT images was reduced to single values representing the mean reflectivity per pixel integrated over the calculated lesion depth. The mean reflectivity per pixel was calculated by dividing the sum of each A-scan in linear intensity units (IU) by the number of pixels in each A-scan. The integrated reflectivity (ΔR) was calculated by integrating the reflectivity in IU units over lesion depth calculated as described above. Two dimensional maps, referred to as collapsed C-scans were produced with each pixel representing the integrated reflectivity over the lesion depth at each pixel.

2.7 Polarized Light Microscopy (PLM)

Polarized light microscopy (PLM) was used for histological examination using a Meiji Techno RZT microscope (Saitama, Japan) with an integrated digital camera, Canon EOS Digital Rebel XT (Tokyo, Japan). Sample sections 200-μm thick are imbibed in deionized water and examined in the brightfield mode with crossed polarizers and a red I plate with 550-nm retardation.

2.8 Digital Transverse Microradiography (TMR)

A custom-built digital TMR system was used to measure mineral loss in the lesion areas. A high-speed motion control system with UTM150 and 850G stages and an ESP300 controller Newport (Irvine, CA) coupled to a video microscopy and laser targeting system was used for precise positioning of the tooth samples in the field of view of the imaging system. The volume percent mineral for each sample thin section was determined by comparison with a calibration curve of X-ray intensity vs. sample thickness created using sound enamel sections of 86.3±1.9 vol.% mineral varying from 50 to 300-μm in thickness using IgorPRO image analysis software. The calibration curve was validated via comparison with cross-sectional microhardness measurements, $r^2 = 0.99$ [24]. Image line profiles 100–150 pixels in width were extracted from the sample ROI representing the percent mineral at each pixel.

3. Results

3.1 NIR images of Suspected Secondary Caries

Near-infrared images of composite restoration margins (n=12) revealed the presence of natural recurrent decay as high contrast optical signals from both wall and outer-type lesions. Polarization sensitive optical coherence tomography (PS-OCT) nondestructively validated the signals obtained in the NIR images through integrated reflectivity (ΔR) collapsed C-scans and profiled the lesions variation with depth from the surface with b-scans. Polarized light microscope (PLM) images of 200-μm cross-sections provided histological evidence of the presence of decay and were utilized to classify the lesion type. Transverse microradiography (TMR) images of the same cross-sections were used as the "gold standard" in determining the presence of recurrent decay and reported the percent mineral of the sample per pixel.

Figure 1 displays the data obtained from a sample with a class I composite restoration presenting a wall and outer dentinal lesion. The restoration margin of this sample was determined to be sound by both examiners via visual examination. All examiners assessed the NIR transillumination image as positive for secondary caries and the NIR reflectance image as negative. PS-OCT and the histology of thin sections over the sample ROI confirmed the presence of demineralization along the wall of the restoration penetrating the outer enamel and dentin. The PS-OCT B-scan displayed in panel H of Fig. 1 shows decay running along the angle of the occlusal restoration that expands considerably at the point where the lesion meets the dentinoenamel junction. This demineralization profile is corroborated exactly by the TMR image shown in panel E. The black line in panel G represents the TMR percent mineral line profile and indicates that the lesion is demineralized to a minimum of approximately 25–30% at the margin. NIR reflectance (blue) and NIR transillumination (red) line profiles extracted from panels B & C respectively, are overlaid with TMR in panel G. Despite being assessed by the examiners as sound, the NIR reflectance image shows an increase in signal coincident with increased demineralization presenting high contrast (0.74) relative to the adjacent enamel and moderate contrast (0.27) contrast value versus the neighboring composite. The NIR transillumination image exhibits a loss in signal from the lesion area with high contrast (0.68) compared to the bordering enamel and moderate contrast (0.18) relative to the composite.

The sample presented in Fig. 2 has another class I composite restoration with a wall and an outer enamel lesion. Similar in location to the lesion depicted in Fig. 1, the margin of the sample in Fig. 2, has demineralization present which was identified by all examiners for visual, NIR reflectance and NIR transillumination. There is a broad lesion that runs across a significant part of the margin while extending into the adjacent enamel. The TMR images shown in panel E and percent mineral line profile (black) in panel G indicate that the mineral content of the lesion profile varies from ~70% mineral in the outer lesion to less than ~30% at the restoration margin. NIR transillumination (panel B), reflectance (panel C) and PS-OCT (panels F & H) each show increased contrast due to demineralization consistent with the PLM and TMR histology. Line profiles extracted from the NIR

reflectance (blue) and NIR transillumination (red) are overlaid with the TMR mineral profile in panel G. The NIR reflectance signal exhibits a maximum intensity at the restoration margin presenting the decay with high contrast compared to enamel (0.47) and moderate contrast (0.35) relative to the composite. The NIR transillumination image exhibits high attenuation across the body of the outer lesion providing high contrast (0.63) versus enamel and poor contrast (0.012) compared to the composite. The PS-OCT B-scan in panel H of Fig. 2 manifests increased scattering at the margin from the wall portion of the lesion, and the adjacent enamel resulting from the outer lesion.

3.2 Secondary caries lesion contrast measurements

For a secondary caries lesion to be easily detected using optical imaging technologies the carious lesion needs to demonstrate high contrast relative to both the adjacent sound enamel and the composite restorative material. To determine if NIR technologies provide significantly higher contrast images of secondary caries compared to visible light, the mean lesion contrast relative to both the adjacent sound enamel and composite restoration was calculated from visible, NIR reflectance and NIR transillumination images of sample restoration margins (Table 1). Compared to the sound enamel, visible images averaged almost no contrast (−0.052) because of their either bright (white spot) or dark (stained) appearance. NIR transillumination demonstrated moderate contrast (0.45) and significantly outperformed visual, and NIR reflectance demonstrated greatest contrast (0.72) and was significantly different from both visible and NIR transillumination. Compared to the composite material, NIR reflectance contrast (0.31) was significantly greater than visible (−0.13) and NIR transillumination (0.13) contrast measurements. Table 1 also shows the range of contrast values calculated for each modality relative to sound enamel and the composite material. For the NIR reflectance measurements relative to the composite, the contrast ranges from −0.71 to 0.73 due to the variety of restorative materials used in natural teeth and their different NIR optical properties.

3.3 Examiner diagnosis of NIR images compared to visual inspection

Histology indicated the presence of secondary caries on all of the teeth selected (12/12). For visual examination the two examiners indicated secondary caries on only 13 out of the 24 assessments (2 per tooth), while for NIR transillumination (19/24) and (11/24) for NIR reflectance. For combined NIR transillumination and reflectance there was at least one positive prediction on 11/12 samples while for visible there was at least one positive prediction for only 8/12 of the teeth.

3.4 Multispectral NIR images of composite restorations in sound teeth

Multispectral NIR occlusal transillumination images centered at 1300-nm, 1460-nm and 1550-nm enhanced the visibility of Z250 composite restorations placed in sound posterior teeth. Figure 3 shows sample NIR images at each wavelength as well as a visible reflectance image with the sample air dried and viewed under 25× magnification (Fig. 3 A). Confidently determining the restorations boundaries with visible inspection remains difficult despite the aforementioned aids. When observed under NIR transillumination (Fig. 3 B,C,D), the restoration boundaries are clearly defined and appear lighter compared to the darker adjacent enamel. Based on the mean contrast values measured from n=16 samples, the Z250

composite manifested the highest contrast for transillumination with 1460-nm (0.55 ±0.16 Fig. C) and 1550-nm (0.59 ± 0.14 Fig. D) light and exhibited significantly lower contrast at 1310-nm (0.10 ±0.12 Fig. B). This is likely due to the reduced water content of the composite material compared to enamel.

4. Discussion

The accurate diagnosis of secondary caries requires the detection of demineralization adjacent to and along the restoration, accompanied with an assessment of the lesion activity [46–48]. This study demonstrates that two-dimensional near-infrared images can show recurrent decay from either wall or outer secondary caries lesions. The agreement between PS-OCT collapsed ΔR C-scans and 2D NIR images (panels C and F in Figs. 1 & 2) are striking in terms of contrast and spatial features. The similarities in 2D NIR imaging and collapsed C-scan OCT data sets suggest that NIR images are suitable for the rapid screening of anterior and posterior teeth. Furthermore, the transparency of enamel and composite to light in the wavelength range between 1300–1700-nm allows evaluation of areas masked by the many commercially available restorative materials demonstrated previously [42].

The advantage of using NIR light at wavelengths greater than 1300-nm, which are not absorbed by the organic molecules responsible for exogenous stains, cannot be overstated. Imaging teeth without the interference of stain will allow a direct assessment of the actual demineralization present in the lesion and prevent false-positive diagnosis based on lesion contrast owing to absorption from stain. This is an important advantage over visual and fluorescence based methods that require clean surfaces and are confounded by stains.

The ability to distinguish between composite, sound enamel and demineralized enamel is necessary for both the detection of recurrent decay and the replacement of restorations with minimal loss of sound tissue structure. The panel of visible and NIR transillumination images in Fig. 3, demonstrate that tooth-color-matched restorations manifest very high contrast with sound tooth structure at NIR wavelengths coincident with high water absorption. NIR light is attenuated to a lesser degree in composite due to the lower water content of composite compared to enamel and dentin.

Ease of interpretation is an important advantage of NIR images for use in detecting dental decay. The natural affinity for such images is supported by the examiner agreement in which this study found NIR images are evaluated more consistently than visual inspection by removing color interpretation and making the comprehension grayscale. This was achieved by clinicians whom have minimal training with this new technology and did not have the ability to view the sample in real time from any angle, which is advantageous for diagnosis and is standard protocol when imaging *in-vivo*.

The main functional limitation when imaging primary caries and secondary caries with NIR imaging technologies is that they rely on light scattering to distinguish between sound and demineralized tooth structure. The complex tooth topography, cracks in dental enamel, and restorative materials with unknown NIR optical properties can all contribute to either masking or generating optical signals that appear as enamel demineralization and can cause false-positive and false-negative diagnoses. Using two-dimensional NIR imaging does well

to overcome these limitations by providing high definition images of the whole tooth surface that enables the clinician to identify if the tooth has any factors that can confound diagnosis.

5. Conclusion

Near-infrared imaging modalities are ideally suited for the detection of demineralization adjacent to and beneath restorative materials due to the high transparency of enamel and dental composites to NIR light. Specifically, NIR reflectance and transillumination imaging are viable methods for the rapid screening of restored tooth surfaces that are capable of detecting early stages of caries lesions.

Acknowledgments

This research was supported by the NIH grants R01-DE14698 and R01DE17869.

References

1. Demarco FF, Correa MB, Cenci MS, Moraes RR, Opdam NJ. Longevity of posterior composite restorations: not only a matter of materials. Dent Mater. 2012; 28:87–101. [PubMed: 22192253]
2. Mjor IA. Clinical diagnosis of recurrent caries. J Am Dent Assoc. 2005; 136:1426–33. [PubMed: 16255468]
3. Kidd E. Diagnosis of secondary caries. J Dent Education. 2001; 65:997–1000.
4. Kidd EA, Beighton D. Prediction of secondary caries around tooth-colored restorations: a clinical and microbiological study. J Dent Res. 1996; 75:1942–6. [PubMed: 9033448]
5. Kidd EAM. Secondary caries. Int Dent J. 1992; 42:127–38. [PubMed: 1500208]
6. Nassar HM, Gonzalez-Cabezas C. Effect of gap geometry on secondary caries wall lesion development. Caries Res. 2011; 45:346–52. [PubMed: 21778722]
7. Fejerskov, O.; Kidd, E. Dental Caries: The Disease and its Clinical Management. Oxford: Blackwell; 2003.
8. Moreira PL, Messora MR, Pereira SM, Almeida SM, Cruz AD. Diagnosis of secondary caries in esthetic restorations: influence of the incidence vertical angle of the X-ray beam. Braz Dent J. 2011; 22:129–33. [PubMed: 21537586]
9. Rudolphy MP, Gorter Y, van Loveren C, van Amerongen JP. Validity of radiographs for diagnosis of secondary caries in teeth with class II amalgam restorations in vitro. Caries Res. 1997; 31:24–9. [PubMed: 8955990]
10. Rudolphy MP, van Amerongen JP, Penning C, ten Cate JM. Validity of bite-wings for diagnosis of secondary caries in teeth with occlusal amalgam restorations in vitro. Caries Res. 1993; 27:312–6. [PubMed: 8402808]
11. Rudolphy MP, van Amerongen JP, ten Cate JM. Radiopacities in dentine under amalgam restorations. Caries Res. 1994; 28:240–5. [PubMed: 8069879]
12. Neuhaus KW, Rodrigues JA, Seemann R, Lussi A. Detection of proximal secondary caries at cervical class II-amalgam restoration margins in vitro. J Dent. 2012; 40:493–9. [PubMed: 22429927]
13. Braga MM, Chiarotti AP, Imparato JC, Mendes FM. Validity and reliability of methods for the detection of secondary caries around amalgam restorations in primary teeth. Braz Oral Res. 2010; 24:102–7. [PubMed: 20339722]
14. Alammari MR, Smith PW, de Josselin de Jong E, Higham SM. Quantitative light-induced fluorescence (QLF): a tool for early occlusal dental caries detection and supporting decision making in vivo. J Dent. 2013; 41:127–32. [PubMed: 22940557]
15. Ando M, Stookey GK, Zero DT. Ability of quantitative light-induced fluorescence (QLF) to assess the activity of white spot lesions during dehydration. Am J Dent. 2006; 19:15–8. [PubMed: 16555651]

16. Pretty I, Smith P, Edgar W, Higham S. Detection of in vitro demineralization adjacent to restorations using quantitative light induced fluorescence (QLF). L Proc Soc Photo Opt Instrum Eng. 2003; 19:368–74.
17. Ando M, Gonzalez-Cabezas C, Isaacs RL, Eckert AF, Stookey GK. Evaluation of Several Techniques for the Detection of Secondary Caries Adjacent to Amalgam Restorations. Caries Res. 2004; 38:350–6. [PubMed: 15181334]
18. Gonzalez-Cabezas C, Fontana M, Gomes-Moosbauer D, Stookey GK. Early detection of secondary caries using quantitative, light-induced fluorescence. Oper Dent. 2003; 28:415–22. [PubMed: 12877427]
19. Konig K, Schneckenburger H, Hibst R. Time-gated in vivo autofluorescence imaging of dental caries. Cell Mol Biol (Noisy-le-grand). 1999; 45:233–9. [PubMed: 10230733]
20. ten Bosch, JJ. Summary of Research of Quanitative Light Fluorescence. In: Stookey, GK., editor. Early detection of Dental caries II. Indianapolis, IN: Indiana University; 1999. p. 261-78.
21. Boston DW. Initial in vitro evaluation of DIAGNOdent for detecting secondary carious lesions associated with resin composite restorations. Quintessence Int. 2003; 34:109–16. [PubMed: 12666859]
22. Lussi A, Megert B, Longbottom C, Reich E, Francescut P. Clinical performance of a laser fluorescence device for detection of occlusal caries lesions. Eur J Oral Sci. 2001; 109:14–9. [PubMed: 11330928]
23. Hitij T, Fidler A. Effect of dental material fluorescence on DIAGNOdent readings. Acta Odontol Scand. 2008; 66:13–7. [PubMed: 18320413]
24. Zanin F, Souza-Campos DH, Zanin S, Brugnera A, Pecora JD, Pinheiro A, et al. Measurement of the fluorescence of restorative dental materials using a diode laser 655 nm. P Soc Photo-Opt Ins. 2001; 2:145–51.
25. Zanin F, Souza-Campos DH, Zanin S, Brughera A, Pecora J, Pinheiro A, et al. Influence of the fluorescence of restorative materials on the detection of secondary caries by 655 nm laser. J Dent Res. 2002; 81:B107-B.
26. Jones, RS.; Fried, D. Proc Soc Photo Opt Instrum Eng. San Jose: SPIE; 2002. Attenuation of 1310-nm and 1550-nm Laser Light through Sound Dental Enamel; p. 187-90.
27. Darling CL, Huynh GD, Fried D. Light Scattering Properties of Natural and Artificially Demineralized Dental Enamel at 1310-nm. J Biomed Optics. 2006; 11:034023 1–11.
28. Simon JC, Lucas SA, Staninec M, Tom H, Chan KH, Darling CL, et al. Transillumination and reflectance probes for near-IR imaging of dental caries. Proc Soc Photo Opt Instrum Eng. 2014; 8929:89290D.
29. Bühler, CM.; Ngaotheppitak, P.; Fried, D. Proc Soc Photo Opt Instrum Eng. SPIE; 2005. Imaging of occlusal dental caries (decay) with near-IR light at 1310-nm; p. 125-31.
30. Li X, King TA. Microstructure and Optical Properties of PMMA/Gel Silica Glass Composites. Journal of Sol-Gel Science and Technology. 1995; 4:75–82.
31. Venz S, Dickens B. NIR-spectroscopic investigation of water sorption characteristics of dental resins and composites. J Biomed Mater Res. 1991; 25:1231–48. [PubMed: 1812117]
32. Stansbury JW, Dickens SH. Determination of double bond conversion in dental resins by near infrared spectroscopy. Proc Soc Photo Opt Instrum Eng. 2001; 17:71–9.
33. Stahl J, Kang H, Fried D. Imaging simulated secondary caries lesions with cross polarization OCT. Proc Soc Photo Opt Instrum Eng. 2010; 754905:1–6.
34. Lammeier C, Li Y, Lunos S, Fok A, Rudney J, Jones RS. Influence of dental resin material composition on cross-polarization-optical coherence tomography imaging. J Biomed Opt. 2012; 17:106002. [PubMed: 23224001]
35. Lenton P, Rudney J, Chen R, Fok A, Aparicio C, Jones RS. Imaging in vivo secondary caries and ex vivo dental biofilms using cross-polarization optical coherence tomography. Dent Mater. 2012; 28:792–800. [PubMed: 22578989]
36. Holtzman JS, Osann K, Pharar J, Lee K, Ahn YC, Tucker T, et al. Ability of optical coherence tomography to detect caries beneath commonly used dental sealants. Lasers in Surg Med. 2010; 42:752–9. [PubMed: 20848554]

37. Simon JC, Chan KH, Darling CL, Fried D. Multispectral near-IR reflectance imaging of simulated early occlusal lesions: Variation of lesion contrast with lesion depth and severity. Lasers in Surg Med. 2014

38. Staninec M, Lee C, Darling CL, Fried D. In vivo near-IR imaging of approximal dental decay at 1,310 nm. Lasers in Surg Med.

39. Wu J, Fried D. High contrast near-infrared polarized reflectance images of demineralization on tooth buccal and occlusal surfaces at lambda = 1310-nm. Lasers in Surg Med. 2009; 41:208–13. [PubMed: 19291753]

40. Fried D, Featherstone JD, Darling CL, Jones RS, Ngaotheppitak P, Buhler CM. Early caries imaging and monitoring with near-infrared light. Dental clinics of North America. 2005; 49:771–93. vi. [PubMed: 16150316]

41. Simon JC, Lucas S, Lee R, Darling CL, Staninec M, Vanderhobli R, et al. near-infrared imaging of natural secondary caries. Proc SPIE Int Soc Opt Eng. 2015; 9306

42. Tom H, Simon JC, Chan KH, Darling CL, Fried D. Near-infrared imaging of demineralization under sealants. J Biomed Opt. 2014; 19:77003. [PubMed: 25036214]

43. Diaz-Arnold AM, Arnold MA, Williams VD. Measurement of water sorption by resin composite adhesives with near-infrared spectroscopy. J Dent Res. 1992; 71:438–42. [PubMed: 1573074]

44. Logan CM, Co KU, Fried WA, Simon JC, Staninec M, And DF, et al. Multispectral Near-Infrared Imaging of Composite Restorations in Extracted Teeth. Proc Soc Photo Opt Instrum Eng. 2014; 8929:89290R.

45. Chan KH, Chan AC, Fried WA, Simon JC, Darling CL, Fried D. Use of 2D images of depth and integrated reflectivity to represent the severity of demineralization in cross-polarization optical coherence tomography. J Biophotonics. 2013

46. Mjor IA, Toffenetti F. Secondary caries: a literature review with case reports. Quintessence Int. 2000; 31:165–79. [PubMed: 11203922]

47. Featherstone, JDB. Clinical Implications:New Strategies for Caries Prevention. In: Stookey, GK., editor. Early Detection of dental caries. Indianapolis: Indiana University; 1996. p. 287-96.

48. Kidd EA, Joyston-Bechal S, Beighton D. Microbiological validation of assessments of caries activity during cavity preparation. Caries Res. 1993; 27:402–8. [PubMed: 8242678]

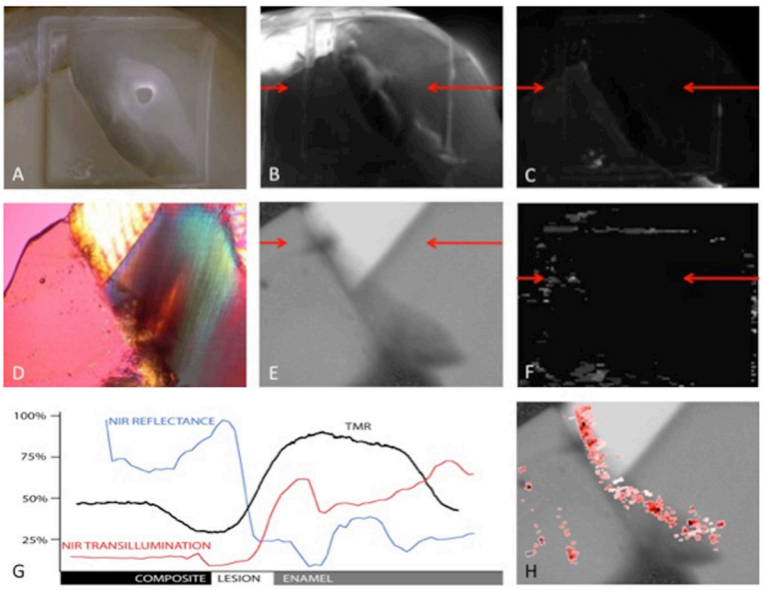

Fig. 1.

(A) High magnification digital image (25× magnification) (B) NIR transillumination image (0.68 contrast vs. enamel & 0.18 contrast vs. composite) (C) NIR cross-polarized reflectance image(0.74 contrast vs. enamel & 0.27 contrast vs. composite) (D) Polarized light microscope image (40× magnification) of 200-μm cross section (E) Transverse microradiography of 200-μm cross section (F) PS-OCT 2D projection of the integrated reflectivity (G) Line profiles (NIR trans-Red, NIR ref-Blue, TMR-Black) normalized from 1–0 (percent mineral for TMR, normalized image NIR pixel values) NIR Line profiles, TMR and PLM cross-section, and PS-OCT B-scan locations are indicated by red arrows. (H) PS-OCT B-scan (red) overlaid with TMR image (gray scale).

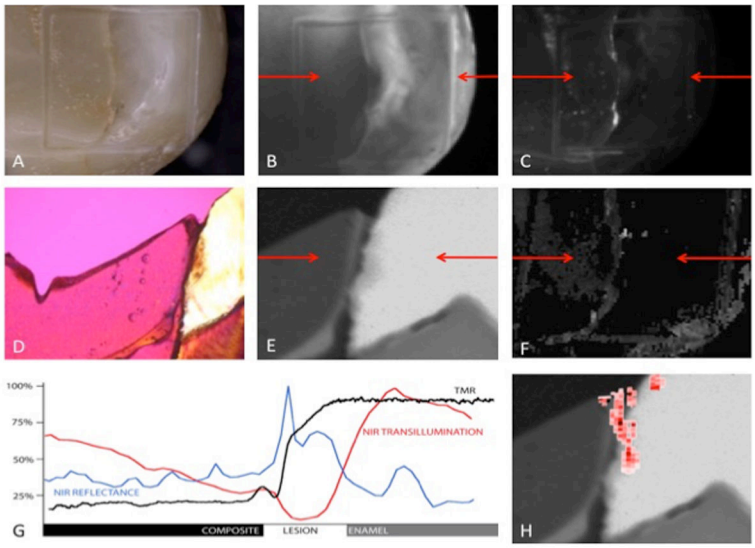

Fig. 2.

(A) High magnification digital image (25× magnification) (B) NIR transillumination image (0.63 contrast vs. enamel & 0.012 contrast vs. composite) (C) NIR cross-polarized reflectance image (0.47 contrast vs. enamel & 0.35 contrast vs. composite) (D) Polarized light microscope image (40× magnification) of 200-μm cross-section. (E) Transverse microradiography of 200-μm cross-section (F) 2D projection of the integrated reflectivity (G) Line profiles (NIR trans-Red, NIR ref-Blue, TMR-Black) normalized from 1–0 (percent mineral for TMR, normalized image NIR pixel values). NIR Line profiles, TMR and PLM cross-section, and PS-OCT B-scan locations are indicated by red arrows. (H) PS-OCT B-scan (red) overlaid with TMR image (grayscale).

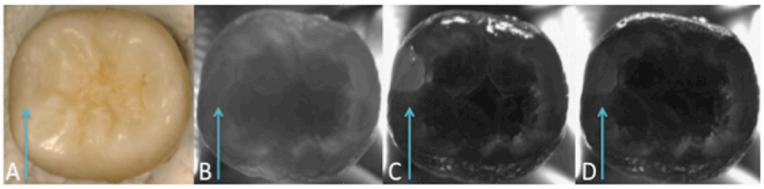

Fig. 3.

Multispectral images of Z250 composite restoration in a sound posterior tooth. (A) Visible light high magnification digital image (25× magnification) (B) NIR transillumination image at λ=1300-nm ±45 (C) λ=1460-nm ±42.5 (D) λ=1550-nm ±20. Blue arrow denotes restoration location.

Table 1

Mean Lesion Contrast Relative to Adjacent Sound Enamel and Composite Restoration

	Mean Contrast	±SD	Min.	Max	Statistical group*
Sound Enamel					
Visible	−0.052	± 0.25	−0.47	0.26	a
NIR reflectance (λ=1500–1700-nm)	0.72	± 0.13	0.49	0.87	b
NIR transillumination (λ=1300-nm)	0.45	± 0.25	0.12	0.75	c
Composite Material					
Visible	−0.13	± 0.27	−0.56	0.20	a
NIR reflectance (λ=1500–1700-nm)	0.31	± 0.40	−0.71	0.73	b
NIR transillumination (λ=1300-nm)	0.13	± 0.16	−0.12	0.44	a,b

*Groups with same letter are statistically similar P > 0.05.